perimental mass resolution had a serious effect on the slope measurements.

[42]See Moffeit, Ref. 36.

[43]See Ballam *et al.*, Ref. 36.

[44]B. L. Ioffe, Zh. Eksp. Teor. Fiz. Pis'ma Red. 9, 163 (1969) [JETP Lett. 9, 97 (1969)]; Phys. Lett. 30B, 123 (1969); H. T. Nieh, *ibid.* 38B, 100 (1972).

[45]H. Cheng and T. T. Wu, Phys. Rev. 183, 1324 (1969); R. W. Griffith, *ibid.* 188, 2112 (1969); H. D. I. Abarbanel and J. B. Kogut, Phys. Rev. D 5, 2050; P. Roy Phys. Lett. 41B, 325 (1972); G. Kramer and H. R. Quinn, Nucl. Phys. B55, 222 (1973); Pham Xuan Yem, Phys. Lett. 41B, 67 (1972).

[46]H. Meyer, in Proceedings of the International Symposium on Electron and Photon Interactions at High Energies, Bonn, 1973 (unpublished).

[47]J. M. Bailey *et al.*, report contributed to the International Symposium on Electron and Photon Interactions at High Energies, Bonn, 1973 (unpublished).

[48]See, for example, J. T. Dakin and G. Feldman, Phys. Rev. D 8, 2862 (1973).

PHYSICAL REVIEW D VOLUME 9, NUMBER 7 1 APRIL 1974

Study of the reaction $p+d\rightarrow \mathrm{He}^3+x^0$

H. Brody,* E. Groves,*† R. Van Berg,* and W. D. Wales*
University of Pennsylvania, Philadelphia, Pennsylvania 19174

B. Maglich,‡ J. Norem,‡§ J. Oostens,‡‖ and M. Silverman¶
Rutgers, The State University, New Brunswick, New Jersey 08903

G. B. Cvijanovich
Upsala College, East Orange, New Jersey 07019

(Received 14 August 1973; revised manuscript received 28 December 1973)

The missing-mass technique has been used to study the spectra of neutral mesons produced by 2- and 3-GeV protons in the reaction $p+d\rightarrow \mathrm{He}^3+x^0$. Cross sections $(d\sigma/d\Omega_{\mathrm{c.m.}})$ of about 10^{-34} cm^2/sr were observed for the π, η, and ω for 3-GeV protons. A peak with a much smaller cross section was observed at a mass of 956 MeV. We have tentatively identified this peak as the η'. Cross sections for the π and η were nearly a factor of 10 larger at 2 GeV than at 3 GeV. Deviations from simple phase space were observed near the two-pion threshold in both 2-GeV and 3-GeV data. Details of the experimental method and of the results are presented.

I. INTRODUCTION

The constraints imposed by the kinematics of two-body interactions facilitate a very attractive experimental method of searching systematically for unstable particles or resonances. The CERN missing-mass spectrometer[1] has demonstrated the great power of a system designed to exploit these constraints. However, the CERN system and its successor, the boson spectrometer,[2] are limited to charged meson states, since they rely on the detection of the proton in the interaction $\pi^-+p\rightarrow p+x^-$. Three of the five well-established nonstrange mesons in the mass range below 1000 MeV (see Table I)[3] have isotopic spin zero and thus cannot be detected by a system similar to the boson spectrometer. In addition there are many other states under 1000 MeV which have been reported but whose existence has not been reliably established. A systematic search for neutral mesons in this mass region is thus easily justified. Although attempts have been made to extend the missing-mass technique to neutral mesons by using the reaction $\pi^-+p\rightarrow n+x^0$, the inherent difficulty in measuring the parameters of the neutron has limited both the resolution and the accuracy of the systematic searches which have been made.

The reaction $p+d\rightarrow \mathrm{He}^3+x^0$ is the simplest accessible reaction which permits precise measurement of the parameters of all three of the known particles in a systematic search for neutral mesons. The experiment was envisioned as the first of a series of endeavors to exploit this reaction and ones similar to it, such as $p+d\rightarrow \mathrm{H}^3+x^+$ (for isotopic-spin-1 particles) and $d+d\rightarrow \mathrm{He}^4+x^0$ (for pure isotopic-spin-0 production). The termination of funding of the Pennsylvania-Princeton Accelerator (PPA) made such investigations impossible.

II. EXPERIMENTAL METHOD

Figure 1 shows the kinematics of the reaction for various mass values of neutral mesons pro-

TABLE I. Established (see Ref. 3) nonstrange mesons below 1 GeV.

Meson	$I^G(J^P)C_n$	Mass (MeV)	Width
$\pi^0(135)$	$1^-(0^-)+$	134.97 ± 0.01	7.8 ± 0.9 eV
$\eta(549)$	$0^+(0^-)+$	548.8 ± 0.6	2.63 ± 0.58 keV
$\rho^0(765)$	$1^+(1^-)-$	765 ± 10	135 ± 20 MeV
$\omega(784)$	$0^-(1^-)-$	783.9 ± 0.3	10.0 ± 0.6 MeV
$\eta'(958)$	$0^+(0^-)+$	957.1 ± 0.6	<4 MeV

duced by 3-GeV protons. When the detected He^3 are restricted to a narrow band of momenta near the maximum allowable kinematic angle, as indicated in Fig. 1, there is an almost linear relationship between the angle at which the He^3 is detected and the square of the mass of the neutral meson. This relationship is shown explicitly in Fig. 2. The figure shows that an accurate measurement of the He^3 angle permits an accurate determination of the mass of the undetected neutral meson.[4] The restriction to the "Jacobian peak" region also maintains approximately the same center-of-mass production angle for the meson over a wide range of laboratory angles. In this experiment, this c.m. angle was about 60°.

A complicating factor was provided by the momentum variation of the PPA proton beam, which was typically about 7%. A momentum uncertainty of this magnitude would destroy the inherently good resolution of the experiment. Since the beam momentum was determined by the magnetic field of the synchrotron, which was itself a well-defined function of time during the spill, it was possible (see Sec. III E 3 for details) to measure the incident proton momentum to about 0.25%. Fortunately, although the kinematics is quite sensitive to the momentum of the incident proton, the laboratory momentum of the He^3 at the Jacobian peak, where the apparatus was set, is very nearly independent of the incident proton momentum. The narrow momentum band shown in Fig. 1 was thus satisfactory for all values of proton momentum. The dashed curve in Fig. 2 shows the relationship between the laboratory angle of the detected He^3 and the square of the missing mass produced by 2.8-GeV protons. The fact that a range of proton momenta was used in a single run provided a valuable check on the consistency of the experiment.

Figure 3 shows a plan view and a side view of the experimental apparatus. The external proton beam of the PPA passed through a liquid deuterium target. The angles of the recoil He^3 were mea-

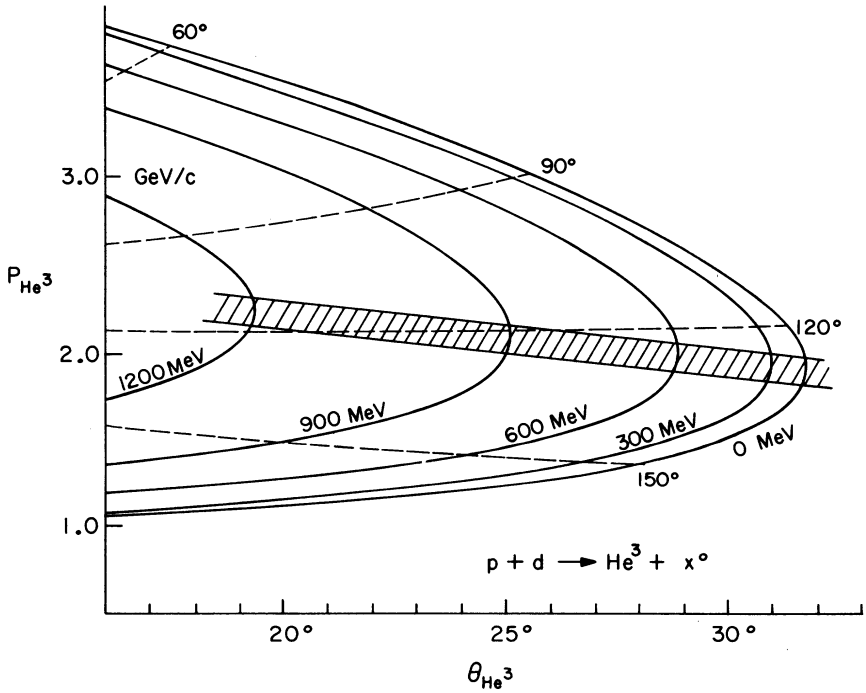

FIG. 1. Kinematics of the reaction $p + d \rightarrow He^3 + x^0$ for 3-GeV protons. The solid curves show the relationship between the laboratory angle and the momentum of the He^3 for constant values of the mass of the neutral meson. The dashed curves indicate constant center-of-mass angles for the He^3. The shaded area is the region investigated by this experiment.

sured with 50-element counter hodoscope. The Jacobian-peak momentum was selected by vertical deflection in a magnet between the target and the counters. Since the magnet deflection was orthogonal to the horizontal angles which were being measured, the production-angle measurement was completely decoupled from the momentum selection.[5]

III. APPARATUS

A. Proton beam

The PPA synchrotron produced a 6–8-msec pulse of protons 19 times a second. This pulse was modulated by the radio-frequency accelerating system to produce 1–2-nsec bursts of protons every 33 nsec. The diameter of the external proton beam at the target was about 1 cm. The divergence of the beam was less than 1 mrad. As mentioned above, the momentum of the protons varied by about 7% during the spill. Details of the system which determined the precise momentum of the proton which produced a specific He^3 detected by the apparatus are given below in Sec. III E 3.

B. Deflecting magnet

The magnet used for the spectrometer was a standard PPA 18D40 bending magnet. The gap, which is normally 6 in. on this magnet, was opened to 8 in. for this experiment. The magnet was mounted on a turntable with the magnetic field horizontal. The horizontal aperture of the magnet restricted the angular acceptance of the system to $\pm 1°$. Since the range of the missing-mass search was from about 20° to 32°, it was necessary to change the equipment configuration to explore the entire mass spectrum. Because the magnet was by far the most massive element in the entire detection system, it proved most convenient to rotate the magnet about its center. The counter system was then moved in an arc about the center of the magnet, and the hydrogen target was moved along the proton beam line. Figure 3 indicates the extreme angular positions of the detection system.

The magnetic field of the magnet was selected to deflect He^3 through 25° in the vertical direction. The fringe field of the magnet was used as a simple converging lens[6] to provide focusing in the horizontal direction. Parallel rays from the target were focused on a plane behind the magnet. Each element of a counter hodoscope set at this focal plane was sensitive only to particles produced at one angle from the hydrogen target. Figure 4 shows the focusing properties of the fringing field.

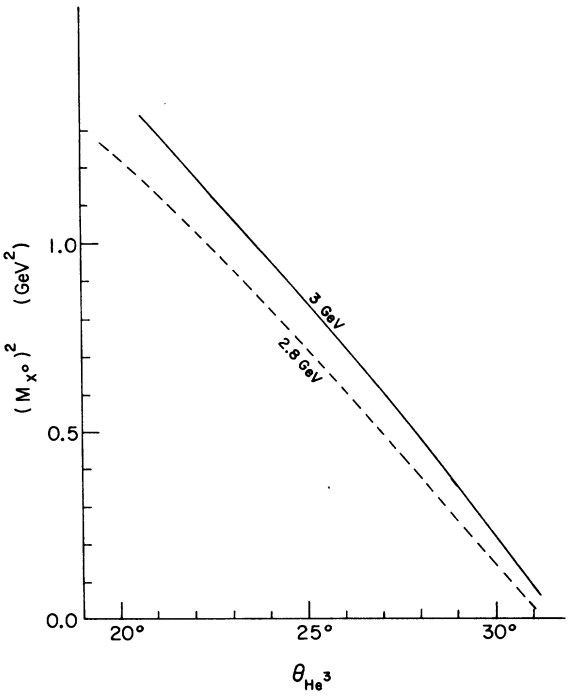

FIG. 2. Square of the mass of the undetected neutral meson vs laboratory angle of the He^3 for the reaction $p+d \rightarrow He^3+x^0$. The solid curve is for 3-GeV incident protons. The dashed curve is for 2.8-GeV protons.

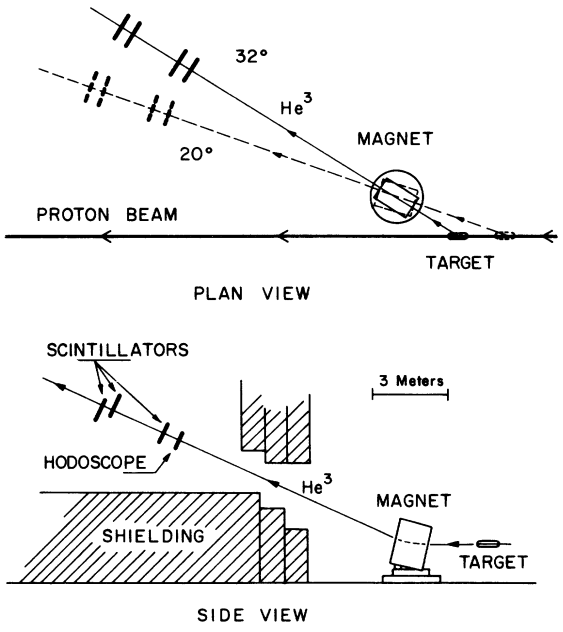

FIG. 3. Plan and side views of apparatus. The shielding has been removed from the plan view to present a clearer picture of the method of changing angles. The two angles shown in the plan view are the extreme angles covered in the experiment. Both views are approximately to scale.

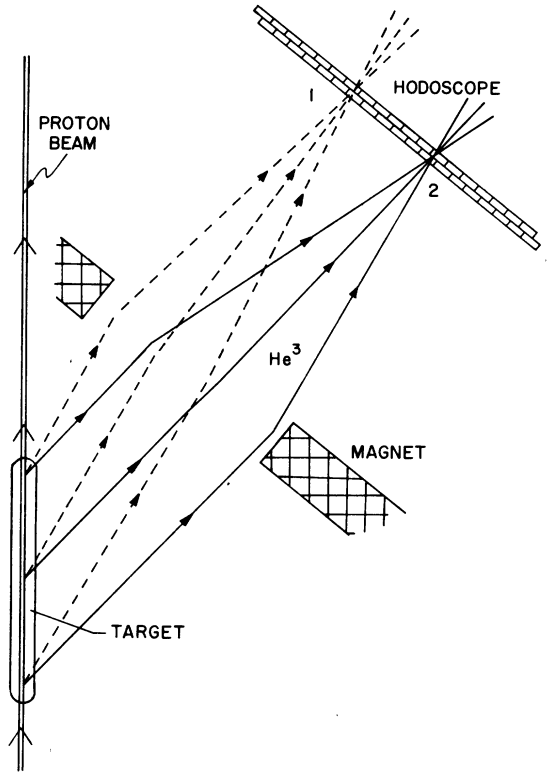

FIG. 4. Focusing properties of magnet and details of hodoscope. He^3 produced at any given angle in the target are focused by the fringe field of the deflecting magnet onto a specific pair of hodoscope elements. The sets of dashed and solid rays (1 and 2) show sample trajectories for two different production angles. The scale has been greatly distorted to permit a clearer display of the focusing effects.

Wire orbit measurements were made to determine the detailed optical properties of the magnet. These measurements indicated the necessity of reducing the vertical aperture at the entrance of the magnet to 2 in. to exclude adverse effects from magnet aberations. When this reduction was made, the wire measurements indicated that parallel rays from the target were focused horizontally to within 0.25 in. at the hodoscope.

C. Target

The target was a thin-walled cylinder made of *H* film, 10 in. long, 1.5 in. in diameter, filled with liquid deuterium, and cooled by a small refrigerator. The target could be moved by remote control in the horizontal direction both along and perpendicular to the beam line. Liquid deuterium could be removed from the target in a few minutes to permit empty target runs. A remotely controlled carbon target was mounted inside the same target system to permit regular calibrations of the detection apparatus. The amount of material through which the emergent He^3 passed was minimized to try to reduce Coulomb scattering. This scattering made the largest contribution to the mass resolution of the apparatus.

D. Detectors

The He^3 detection equipment consisted of three large scintillation counters and a 50-element hodoscope mounted on a large rack that could be rotated through the angular range needed in the experiment. The vertical aperture at the entrance of the magnet and the overlap between the two offset rear scintillators determined the momentum spread of the He^3 accepted by the apparatus. This momentum acceptance ($\Delta P/P$) varied from about $\pm 3.5\%$ at 20° to nearly $\pm 4.5\%$ at 32°. The rack was constructed of steel "*I*" beams and could be rolled on an iron track in an arc centered at the magnet. Angle marks were scribed on the floor with a resolution of approximately 10 millidegrees. One man could easily roll the entire assembly to the prescribed angle and secure it in place with kick-jambs. The three large scintillators, each 27 in. high, 44 in. wide, and 0.25 in. thick, were made of Nuclear Enterprises NE110 scintillator material, and each was viewed with four Amperex 58 AVP 5 in. phototubes. The signals from the four tubes, after being suitably delayed and equalized, were added to produce a single signal. This technique assured uniform light-collection efficiency over the large counter area and a minimum of time-slewing of the signal from various parts of the counter. The light-collection uniformity was of prime importance since the He^3 were discriminated from other particles primarily on the basis of their energy loss in the scintillators. Special phototube bases were designed to ensure that the pulse height was linear over a large dynamic range, even under high-count-rate conditions. This was accomplished by supplying the top ten dynodes of each tube base from one high-voltage supply and each of the bottom four dynodes of these tubes from separate 300-V supplies. A Ferranti XP 21 light-emitting diode was glued to the center of each scintillator to produce light pulses which were used for timing and equalization of the phototubes.

The hodoscope was made of 50 overlapping pieces of scintillator 22 in. high, 1.485 in. wide, and 0.25 in. thick. A UVT Plexiglas strip glued on one end of each scintillator routed the light to a 56 AVP phototube. These pieces were mounted in two planes with 1.500 in. spacing between centers of scintillator elements. The two planes were then mounted parallel with a 0.750-in. offset (see Fig. 4). This structural arrangement provided

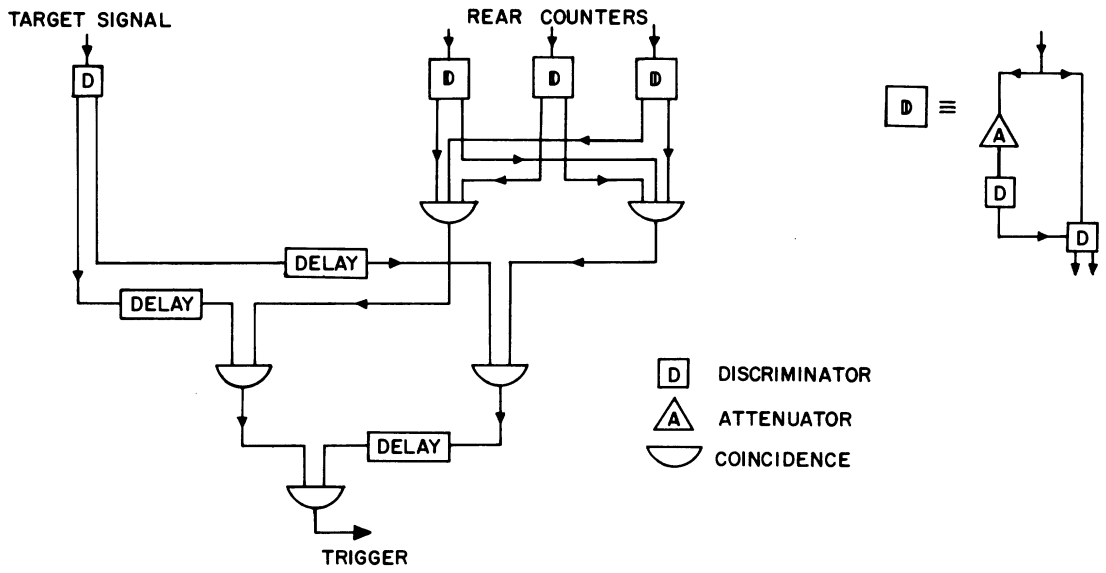

FIG. 5. Fast-logic diagram. Three separate time-of flight measurements (between the target and the first rear counter, the target and the last rear counter, and the first and last rear counters) were made. Attenuators in the signal lines from the three rear counters permitted elimination of pulses due to particles with lower ionization than He^3.

49 hodoscope elements composed of unique coincidences between members of the front plane and adjacent overlapping offset members of the back plane. The coincidence structure was selected to improve rejection of spurious proton- or pion-induced events in the hodoscope.

Two PEK 118-nanosecond pulsed-light sources were installed in the hodoscope as a further aid in testing the operation and relative timing of hodoscope members. Each member of a plane was connected to one of these lamps by about a yard of Edmond Scientific Corp. plastic fiber light guide. Pulsing the lamp produced a simultaneous light pulse at the 25 hodoscope members of one plane to permit convenient timing of the system.

To further reduce the coulomb scattering and interactions of the He^3 a helium-filled polyethylene bag was placed in the beam path from the deuterium target to the hodoscope.

E. Electronics

The electronic equipment associated with the experiment performed three functions: (1) identification of a He^3, (2) measurement of the angle of emission of the He^3, and (3) determination of primary proton beam energy at the time of He^3 detection.

1. He^3 *identification*

The He^3 were identified using pulse height (relative ionization) in the three large scintillation counters and by time of flight. Since the He^3 are doubly charged, they produce an ionization which is four times that amount which would be produced by a singly charged particle of the same velocity. At the momenta selected for this experiment, the He^3 produced eight times the minimum ionization. The sensitivity of the counter system was reduced to accept only particles whose ionization was more than five times the minimum. A separate scintillation counter which was not required in any of the trigger logic was used as a pulse-height monitor. This counter was located behind all the other scintillators and clearly indicated that no particles of ionization less than that expected for He^3 were leaking through the trigger logic. Since the PPA external beam was modulated by the rf into 1-nsec bunches every 33 nsec, it was convenient to measure the time of flight from the deuterium target to a counter in the equipment. The accelerator provided a signal in synchronization with the beam rf bunches which was used in the time-of-flight measurements. The fast logic is diagrammed in Fig. 5. The inset to the figure shows the discrimination and attenuation system used with each of the large counters. The signal from the counter was split, and one side was attenuated prior to the first discriminator. The output of this discriminator was used as input for a second discriminator which was exposed to the unattenuated signal from the other side of the split. The timing of this second discriminator was then not influenced by the attenuation necessary to determine pulse-height levels.

Two separate coincidences were made which

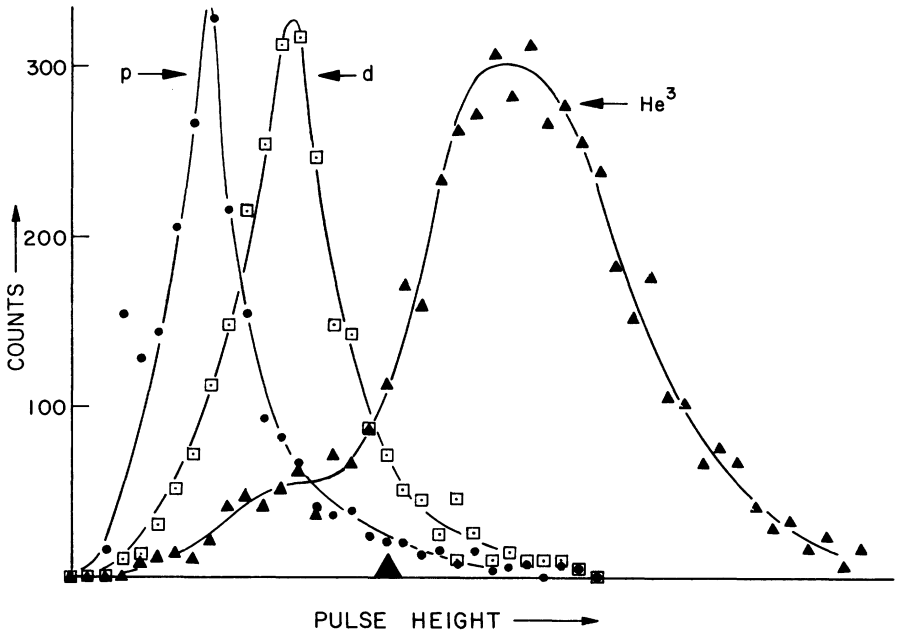

FIG. 6. Pulse-height spectra. The time-of-flight requirements were set sequentially to protons, deuterons, and He^3, and the output signal from one of the rear counters was fed to a pulse-height analyzer whenever these requirements were satisfied. The curves are freehand fits to the data points. The He^3 spectrum was taken with the attenuators in the other two rear counters set to discriminate against protons and deuterons. The shoulder on the left-hand edge of the He^3 curve represents deuterons leaking through the system. The discontinuity on the left-hand edge of the proton curve probably represents a fault in the analyzer operation. The triangle on the horizontal axis of the graph shows the point at which the threshold was set for normal counting of He^3.

required all of the three large rear counters. The output of one coincidence, which was in time with the signal from the first rear counter, was used to define the time of flight between the first rear counter and the target. The output of the second coincidence circuit, which was in time with the last rear counter, was used to define the time of flight between the last rear counter and the target. Finally, the outputs of these two coincidences were used to define a third time of flight between the first and last rear counters. The redundancy of the system was mandated by the fact that the proton and deuteron rates through the apparatus were several orders of magnitude higher than the He^3 rate. Figure 6 indicates the discrimination which was achieved. The three spectra show the pulse heights from one counter when protons, deuterons, and He^3 were selected by the time-of-flight system.

2. *Angle measurement*

Counter-coding units designed by T. Droege of PPA performed a coincidence between the overlapping front- and back-row counters whenever a He^3 trigger was present. The output of the counter-coding units was fed directly into one side of the memory of a Nuclear Data Model 160 two-dimensional analyzer. Figure 7 shows a schematic diagram of the data-recording logic. Triggers in which two particles meeting the pulse-height and coincidence requirements passed through the hodoscope simultaneously were rejected. Triggers where no particle met these requirements were also rejected. Rejected triggers were scaled as a check on the apparatus performance. Typically the rejection rate was between 5% and 10%.

3. *Proton beam energy*

The energy of the primary proton beam at PPA varied by approximately 7% during the course of the spill. The energy was determined by measuring the magnetic field of the synchrotron at the instant an interaction took place. The output of a coil which was placed in the synchrotron field gave the time derivative of the field. This signal was integrated in a stable high-precision integrator and the output sampled at the time at which a He^3 trigger was received. This sampled voltage was digitized and fed into the other side of the two-dimensional pulse height analyzer, as indicated in Fig. 7. An attempt was made to monitor the peak energy of the external proton beam by measuring the internal rf frequency of the machine during the beam spill. This did not provide the

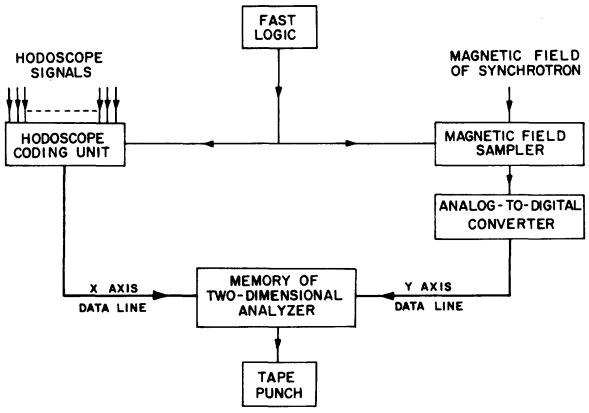

FIG. 7. Data-recording logic. A trigger from the fast logic (see Fig. 6) actuated units connected to the hodoscope outputs and to a signal proportional to the magnetic field of the synchrotron. The hodoscope coding unit produced a digital signal corresponding to the number of the hodoscope element through which the He^3 had passed. This digital information was then transmitted to the "X" data line of the memory of a two-dimensional analyzer (Nuclear Data Model 160). The magnetic-field sampler produced a signal proportional to the magnet field of the synchrotron at the instant the event occurred. This signal was passed through an analog-to-digital converter and then to the "Y" data line of the analyzer memory. At the end of each run the contents of the memory were punched on paper tape for further analysis.

accuracy needed, because of slight variations in the orbits of the protons within the synchrotron, so the final value of the proton beam energy was determined by using the observed angles of π, η, and ω meson production.

Since the angle of the He^3 is directly related to the (missing mass)^2 of the meson produced, the two-dimensional analyzer may be thought of as storing approximately 25 different missing-mass spectra, one for each of the incident-momentum bins into which the PPA energy was divided. The fact that it was possible to perform simultaneously many different missing-mass experiments at slightly different bombarding energies allowed us to test the invariance of the mass of a peak with respect to changes in the incident momentum.

IV. RUNNING PROCEDURE

A. Data collection

The hodoscope, magnet, and target were rotated and translated to the angle corresponding to a selected mass region. The hodoscope position could be read to a hundredth of a degree. Although the magnet angle was known only to a tenth of a degree, the optics of the magnetic focusing make the measurement of missing mass insensitive to small misalignment of the magnet. The magnet current was set to select the momentum in the Jacobian-peak band. A carbon target was inserted in the beam to give a high counting rate for He^3. (The He^3 rate from carbon was more than an order of magnitude greater than the rate from an equivalent amount of deuterium). Time-of-flight spectra were taken and all three timing circuits set on the He^3 peak. The discriminators on all three large counters were checked to ensure that they were not cutting off He^3. A run was taken to check that the angular distribution of He^3 from carbon was smooth, to ensure that each hodoscope element had the same efficiency.

The carbon target was then removed and the liquid deuterium target inserted. A series of target-full and target-empty runs were taken. The hodoscope was then shifted a small (noninteger number of elements) distance and more full and empty runs were taken. For a given magnet and target angle setting, three to five slightly different hodoscope settings were used to eliminate the possibility of spurious holes and peaks. After sufficient data were accumulated, the entire system was moved to a new angle and the complete procedure repeated.

Runs were taken over the entire range of angles which were accessible to the equipment. Typical target-full runs lasted three hours, with a counting rate averaging 10^4 He^3 per hour. The empty-target rate was 20–60% of the target-full rate, depending upon the angle being run. At the completion of each run the contents of the memory of the two-dimensional analyzer were punched on paper tape for later analysis.

B. Monitors and calibrations

The proton beam passing through the liquid target was monitored with two counter telescopes. The counting rate from a solid-state detector which looked at a thin target upstream from our target was also monitored. The accelerator provided a monitor which measured the voltage induced on a tuned cavity through which the beam passed. The latter two monitors were necessary when empty-target runs were done. None of these monitors was stable over the long term to better than ±25%. Ratios of the various monitors were computed and were found to form blocks of fairly uniform (±5%) ratios separated by discontinuities corresponding to changes in machine parameters. An examination of all these monitors early in the experiment indicated that the gross He^3 rate in the apparatus had much more long-range stability than any of the monitors used. In addition, the He^3 rate, when averaged over all the hodoscope angles accessible at a given magnet angle setting,

was found to depend linearly upon magnet angle. The He^3 rate vs magnet angle was fitted using the least-squares method to each of the blocks of monitor stability. This rate was used to bridge the discontinuities in the performance of our monitors. Although this procedure is conceptually distasteful, it does not appear to have introduced any major systematic errors into the experiment.

All the monitors were calibrated with a foil irradiation. This was done several times during the experiment by measuring the Na^{24} activity induced by the external beam protons in a 0.000 35-in. Al foil due to the reaction $Al^{27}(p, 3pn)Na^{24}$. The cross section used for this activation is 10 ± 1 mb. Counting statistics are better than 3%. Dr. W. Schimmerling of the PPA staff, from whom this information comes, estimates that the overall accuracy of the intensity measurements is 15%. This estimate sets a 15% limit on the absolute values of our measured cross sections at 3 GeV. The calibration of the monitors for the 2-GeV data was much less thorough. Consequently, the absolute values for the cross sections at 2 GeV may be in error by as much as 25%.

The angular limit set by the magnet apertures was smaller than the angle covered by the hodoscope counters. Accordingly, the rate in each hodoscope element depended strongly on how much of the total target volume was shadowed by the magnet aperture. Since the knowledge of this variation in the hodoscope response was obviously critical to the analysis of the data, several different approaches were made:

(1) The relative counting rates were calculated from knowledge of the target size, the beam size, the magnet apertures, and the focusing system.

(2) A dummy target of styrofoam was constructed and used to check these calculations.

(3) The empty target was occasionally translated during the experimental run to permit the proton beam to transverse the cylinder wall. The data from the 0.003-in. H-film wall gave the relative rates from a long target.

(4) The data from the carbon target (effectively a point source) were used to calculate the expected rates from a long target.

The results of all these methods were in rough agreement. The geometrical corrections actually applied to the counting rates were those calculated directly. A typical correction function is shown in Fig. 8.

V. RESOLUTION

The experimental resolution of measurement of the mass (M_4) was determined by the accuracy of

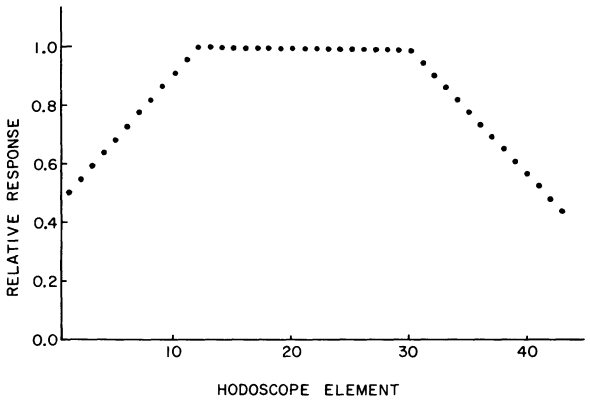

FIG. 8. Relative response of hodoscope. The central plateau shifted from one end of the hososcope to the other as the counters were shifted relative to the central angle determined by the positions of the magnet and target.

the measurement of the laboratory momentum of the He^3 (P_3), the laboratory momentum of the proton (P_1), and the laboratory angle of the He^3 (θ_3). The contribution of the errors in each of these measurements can be calculated by examining the relationship between the missing mass and the appropriate parameters measured in the laboratory system:

$$M_4^2 = (E_1 + M_2 - E_3)^2 - P_1^2 - P_3^2 + 2P_1P_3\cos\theta_3 .$$

The square of the error in the mass determination is then

$$(\Delta M_4^2)^2 = \left(\frac{\partial M_4^2}{\partial P_3}\Delta P_3\right)^2 + \left(\frac{\partial M_4^2}{\partial P_1}\Delta P_1\right)^2 + \left(\frac{\partial M_4^2}{\partial \theta_3}\Delta\theta_3\right)^2 . \quad (1)$$

The effect of errors in the measurement of P_3 was minimized by the Jacobian-peak design of the spectrometer. The contribution of the first term in (1), averaged over the apparatus momentum bite, varies between ± 0.0068 and ± 0.0075 GeV^2 for 3-GeV protons.

The second term in (1) was due primarily to short-term fluctuations in the external proton beam momentum. ΔP_1 is estimated to be ± 10 MeV/c, contributing between ± 0.003 and ± 0.007 GeV^2 at 3 GeV.

The error in θ_3 is due primarily to multiple scattering of the He^3 in the deuterium target. Multiple scattering elsewhere along the flight path, imperfections in the magnetic fringe field focusing, and the finite width of the hodoscope elements also made non-negligible contributions. $\Delta\theta_3$ from multiple scattering before the magnet (excluding that from the target) is ± 0.0012 rad. $\Delta\theta_3$ from multiple scattering after the magnet is ± 0.001 rad.

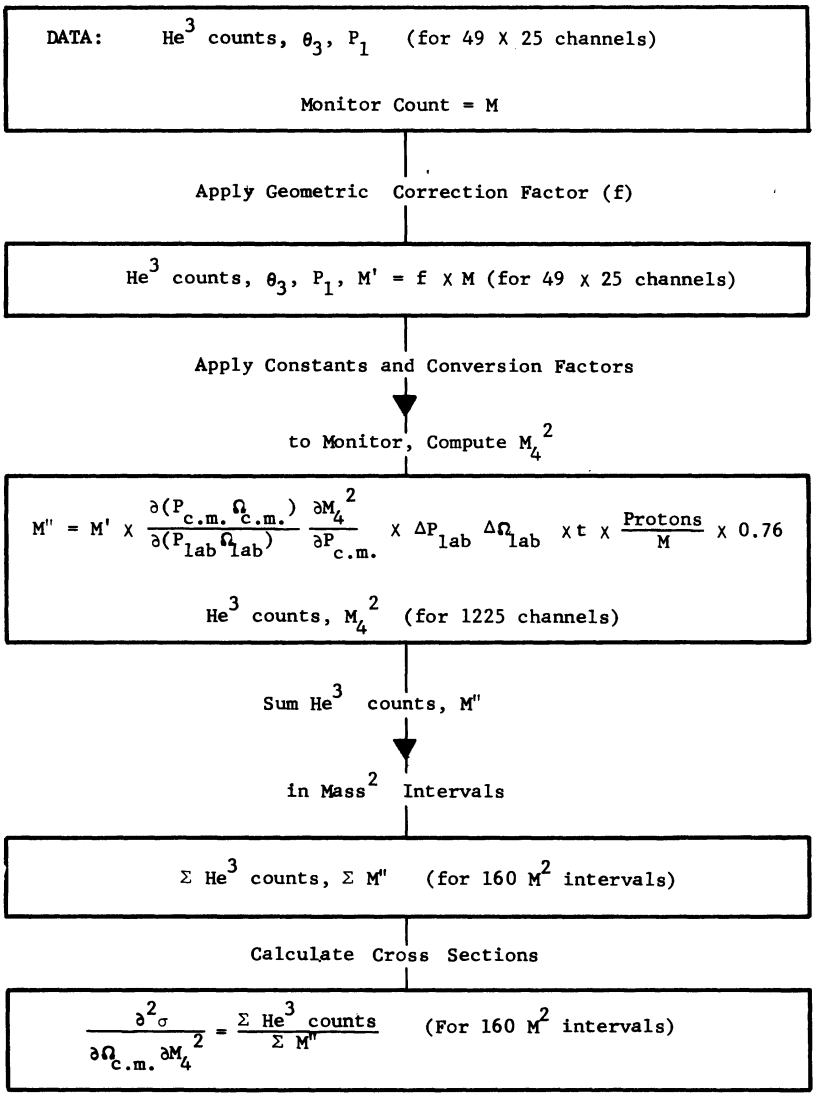

FIG. 9. Summary of data analysis and cross section calculation.

Fuzziness due to poor focusing and to hodoscope element width contributes $\Delta\theta_3$ of ±0.0003 and ±0.0011 rad, respectively. Multiple scattering in the target varied with the beam position and fluctuated between ±0.002 and ±0.0018 rad. Multiple scattering of the protons in the target and proton beam divergence contributed ±0.0008 and ±0.000 75 rad, respectively. Adding all of these in quadrature yields an effective $\Delta\theta_3$ of ±0.0029 rad. The third term of (1) is then ±0.023 GeV^2 at 0.018 GeV^2 and ±0.021 GeV^2 at 0.60 GeV^2 for 3-GeV protons. The sum of these factors produces a resolution which varies between ±0.024 and ±0.025 GeV^2 at a $(mass)^2$ of 0.018 GeV^2 and between ±0.022 and ±0.023 GeV^2 at 0.60 GeV^2 for 3-GeV protons. The corresponding mass resolution is readily calculated from the relationship

$$\Delta M \cong \frac{\Delta(M^2)}{2M}$$

and varies from about ±90 MeV at a mass of 135 MeV to about ±15 MeV at a mass of 785 MeV.

Similar calculations for 2-GeV protons give values of ±0.018 GeV^2 at 0.18 GeV^2 and ±0.017 GeV^2 at 0.301 GeV^2. The corresponding mass resolution varies from about ±65 MeV at a mass of 135 MeV to about ±16 MeV at a mass of 585 MeV.

VI. ANALYSIS PROCEDURE

A. Data reduction

The data for each individual run consisted of hodoscope spectra for each of 25 different proton momentum intervals. These data and the monitor

information for each run were processed on the PPA PDP-10 facility. Each hodoscope spectrum was corrected by multiplying the monitor count by the appropriate geometrical factor (see Fig. 8). A new monitor count was then associated with the He^3 count in each hodoscope element. The $(\text{mass})^2$ corresponding to the incident proton momentum and angular positon of each element was then calculated. At the same time, the appropriate constants and transformation factors were incorporated into the monitor count. At this point, the sums of He^3 counts and monitor counts corresponding to any specific mass interval could be made for a single run or for a selected set of runs. The He^3 sum, when divided by the monitor sum, gives the production cross section. Figure 9 may make the logic of the operation somewhat more clear.

The target thickness, t, was 12.6×10^{23} deuterons/cm^2. The product of solid angle and momentum acceptance was between 3 and $4.5\times P_3$ (μsr GeV/c) for the angular range used. The factor of 0.76 is the fraction of He^3 which survive cutoffs on pulse height and time of flight (95% for each) and are not lost due to interactions in the material before the final detector (85%).

The final cross section presented, $d^2\sigma/d\Omega_{\text{c.m.}}\,dM_4^2$, was selected because of its similarity to the actual measured laboratory distributions and because it is easy to relate to phase-space distributions.

This particular method of analyzing the data preserves the actual count, and hence the counting statistics, to a very late stage in the operation. The program could calculate cross sections for individual runs or selected sets of runs, and could subtract corresponding empty-target cross sections. The program also had an option which permitted selection of a subset of the total number of incident-proton momentum intervals for analysis. The results of this type of analysis for all of the 3 GeV data are shown in Fig. 10.[7]

B. Fitting procedure

Although the data shown in Fig. 10 contain several very obvious peaks, the computation of exact masses and cross sections requires that the data be matched to a fitting function. The function used to fit the data, after empty-target rates were subtracted, is

$$F(M_4^2)=\frac{1}{\sqrt{2\pi}\,a}\int_{-\infty}^{\infty} e^{-(M_4^2-M_4'^2)^2/2a^2}\,g(M_4'^2)\,dM_4'^2,$$

where the convolution integral is used to include the effect of the experimental resolution. Here a

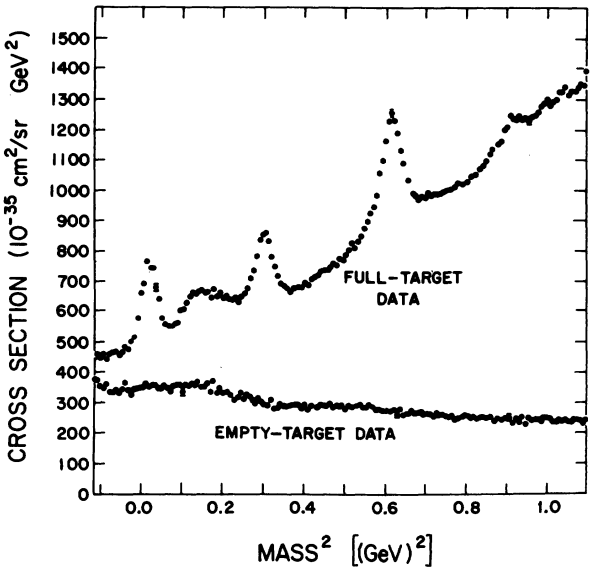

FIG. 10. All data for incident 3-GeV protons. The upper curve shows the differential cross sections from the full deuterium target, while the lower curve shows the background rates when the deuterium was removed from the target. Errors have been included for only a few typical data points.

is the half-width of the experimental resolution, and

$$g(M_4'^2)=b_i h_i(M_4'^2).$$

The b_i's are adjustable constants, and the h_i are indicated below:

$h_1=1$, constant term

$h_2=2\pi$ invariant phase space (see Ref. 8),

$h_3=3\pi$ invariant phase space,

$h_4=4\pi$ invariant phase space,

$$h_5=\begin{cases}(M_4'^2-M_{5\pi}^2), & M_4'\geq M_{5\pi}\\ 0, & M_4'<M_{5\pi}\end{cases}\quad\text{polynomial}$$

$$h_6=\begin{cases}(M_4'^2-M_{5\pi}^2)^2, & M_4'\geq M_{5\pi}\\ 0, & M_4'<M_{5\pi}\end{cases}\quad\text{polynomial}$$

$$h_7=\begin{cases}(M_4'^2-M_{5\pi}^2)^3, & M_4'\geq M_{5\pi}\\ 0, & M_4'<M_{5\pi}\end{cases}\quad\text{polynomial}$$

$h_8=\delta(M_4'^2-M_\pi^2)$, π term, M_π a variable

$h_9=\delta(M_4'^2-M_\eta^2)$, η term, M_η a variable

$h_{10}=\frac{M_\omega \Gamma_\omega \pi^{-1}}{(M_4'^2-M_\omega^2)^2+\Gamma_\omega^2 M_\omega^2}$, simple Breit-Wigner distribution for ω; Γ_ω, M_ω variable

$h_{11}=\frac{M_\rho \Gamma \pi^{-1}}{(M_4'^2-M_\rho^2)^2+\Gamma^2 M_\rho^2}$, Selleri-modified[9] Breit-Wigner distribution

$M_\rho \equiv 765$ MeV, $\Gamma=\Gamma_\rho\left(\frac{q}{q_0}\right)^3\frac{2q_0^2}{q_0^2+q^2}$, Γ_ρ variable,

q = 3-momentum of decay pion in the M_4 c.m. system,

q_0 = 3-momentum of decay pion in the $\rho(765)$ c.m. system,

$h_{12}=\frac{2}{W}\exp\left[+\frac{(M_4^2-M_4'^2)^2}{2a^2}-\frac{(M_4'^2-M_x^2)^2}{2W^2}\right]$, Gaussian fit for bump at 0.9 GeV^2; M_x, W variable.

An examination of the terms used may make the rationale for the fitting function somewhat more obvious.

The most serious problem in calculating the resonance parameters is the exact shape of the nonresonant background upon which they are superimposed. The data of Fig. 10 show clearly that the cross sections are not zero below the pion mass or between the pion and the start of two-pion phase space. We have assumed a constant term (h_1) in the background to account for this fact. This assumption is discussed in more detail in Sec. VII. We made the initial hypothesis that the background below five-pion masses would be fitted well by a sum of two-, three-, and four-pion phase spaces (h_2, h_3, and h_4). This seems to agree fairly well with the data. Above 5π masses the contributions from multiparticle phase spaces become very complex but seem to contribute a smoothly rising background. We fitted this increase in background with a third-order polynomial (h_5, h_6, and h_7). Unfortunately, this background fitting procedure can mask broad resonances. However, it cannot create narrow resonances.

The peaks corresponding to the π and the η were fitted with delta functions (h_8 and h_9), whose position was permitted to vary to optimize the fit. The peak corresponding to the ω was fitted with a simple Breit-Wigner shape (h_{10}), with both the resonance width and position varied to optimize the fit.

Although the presence of the ρ is not obvious from this data in Fig. 10, we reasoned that such a broad resonance might not be strikingly evident with the high background in the region and with the ω superimposed on it. Accordingly, we put a Selleri-modified[9] Breit-Wigner shape (h_{11}) into the fit, with the mass fixed at the known ρ mass and the width varied to optimize the fit.

The data seem to indicate the presence of a rather narrow peak at about 0.9 GeV^2. Initial fits with a normal Breit-Wigner shape gave inconsistent cross sections, probably because the peak seems narrower than our calculated resolution. An improvement was made by fitting the data to a simple Gaussian shape (h_{12}) and then calculating the resonance width by hand after the fitting had been optimized.

Figure 11 shows the terms used in the fitting program at 3 GeV. Figure 12 shows the data and fit for each of three P_1 intervals near 3.8 GeV/c and for the total data taken at that energy. Figure 13 shows the data and fit for the data taken at 2 GeV. The better resolution and significantly higher cross sections at the lower energy are evident from the data. The excellent agreement of the data and the fitted curves at the positions of the π, η, and ω show that the experimental resolution of the apparatus was very close to the calculated resolution. Table II shows the parameters which provided the optimum fits. The errors shown in the table are statistical only, and do not

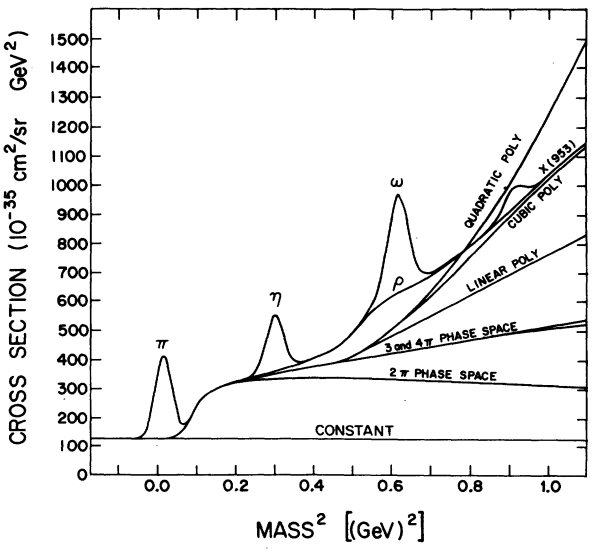

FIG. 11. Differential cross section of terms used in fitting mass distribution for 3-GeV data.

reflect any systematic errors, which are discussed in detail below.

VII. DISCUSSION

As mentioned in Sec. III, there is an uncertainty of about 15% in the absolute proton intensity calibration, and hence a corresponding systematic error of the same order of magnitude in all measured cross sections. The corrections for He^3-counting efficiencies and for interaction losses are not well known, and probably contribute an over-all uncertainty of 5% to the measured cross sections. The acceptance of the system ($\int P d\Omega$) has been calculated from the measured parameters of the spectrometer system. The absolute error in this calculation is probably about 10%. In addition, since the parameters of the system changed a great deal (due primarily to the translation of the target along the beam line) as the angle of the spectrometer system was changed, there is an estimated 5% relative error in the acceptance used. Finally, the somewhat *ad hoc* nature of the fitting routine does not inspire confidence in the errors cited in Table II.

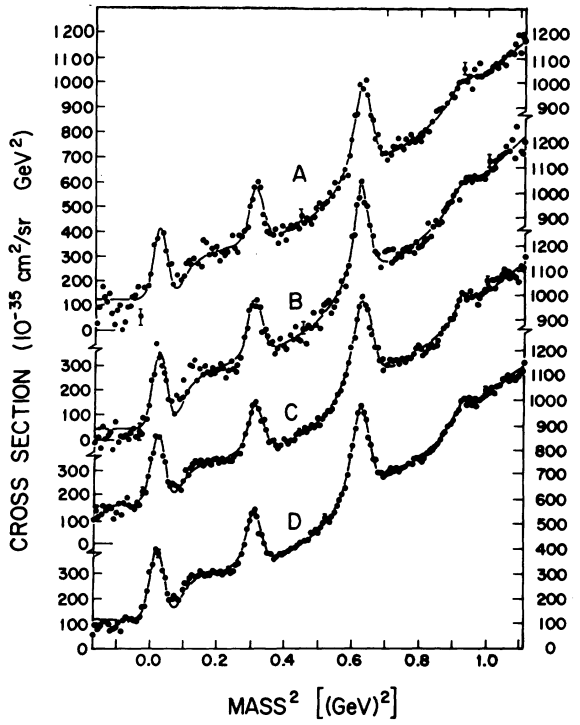

FIG. 12. Differential cross sections from deuterium at 3 GeV. The empty-target cross sections have been subtracted. The curves are the best fit to the data. Curve *A* is for incident proton momenta from 3.71 to 3.77 GeV/*c*, curve *B* is for momenta from 3.77 to 3.81 GeV/*c*, curve *C* is for momenta from 3.81 to 3.85 GeV/*c*, and curve *D* is for the total 3 GeV data, for momenta from 3.71 to 3.85 GeV/*c*. Typical statistical errors are shown. The smaller errors in the data at higher incident proton momentum reflect the fact that the proton intensity from the synchrotron is peaked at the maximum momentum.

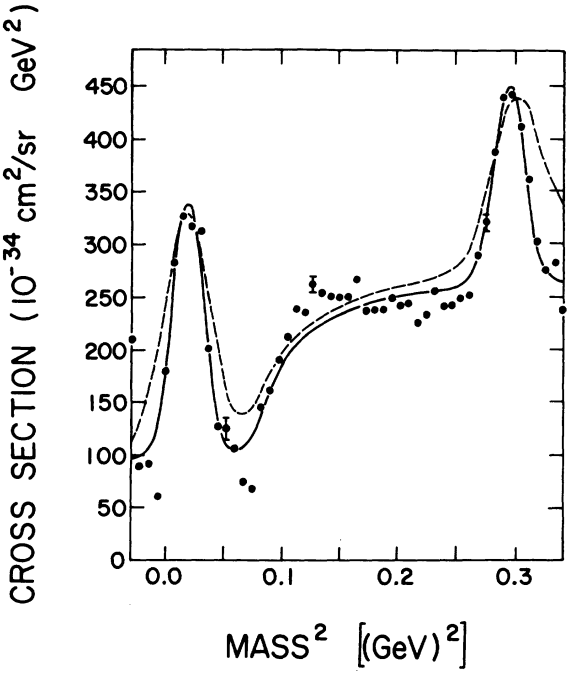

FIG. 13. Differential cross sections from deuterium at 2 GeV. The solid curve is the fit to the data. The dashed curve, for comparison, is ten times the fit to the total 3 GeV data.

One of the least satisfying features of the fit is the use of a constant term in the background spectrum. (In all of the discussion below, "background" refers to the nonresonant part of the data which remained after the empty-target data had been subtracted.) This term is roughly half the total cross section in the 2π threshold region. Our assumption of a constant term is probably naive. However, being unable to experimentally investigate all of the background sources, we were not able to determine the exact shape of this part of the background. Possible mechanisms which might produce such a background are principally the following:

(1) elastically scattered protons making He^3's in the target walls and the magnet pole faces;

(2) He^3's scattering in the magnet pole faces;

(3) He^3's produced by secondaries within the target, e.g.,

$$p+d \rightarrow p+d\,,$$

$$d+d \rightarrow He^3+n+x^0;$$

TABLE II. Cross sections and widths of resonances observed. The errors shown are purely statistical and depend, in some instances, on details of the fitting program. A more realistic estimate of the errors is shown in Table III.

Incident proton momentum (GeV/c)	Meson observed	Mass^2 (GeV^2)	Mass (MeV)	Full width at half maximum (MeV)	$d\sigma/d\Omega_{c.m.}$ (10^{-36} cm^2/sr)
3.71–3.77 (3 GeV; low sample)	π	0.020 ±0.002	141±7	0.0[a]	158 ±10
	η	0.298 ±0.002	546±2	0.0[a]	114 ±8
	ω	0.6113±0.008	782±1	6.3±1.2	204 ±16
	ρ	0.59[a]	768[a]	166 ±21	672 ±104
	η'	0.908 ±0.007	953±4	23 ±6	40 ±10
3.77–3.81 (3 GeV; middle sample)	π	0.0182±0.0016	135±6	0.0[a]	142 ±10
	η	0.3003±0.0034	548±3	0.0[a]	104 ±6
	ω	0.6141±0.0009	784±1	12.5±1.1	249 ±3
	ρ	0.59[a]	768[a]	180 ±35	662 ±6
	η'	0.906 ±0.007	953±4	23 ±8	46 ±12
3.81–3.85 (3 GeV; high sample)	π	0.0194±0.0006	139±2	0.0[a]	154 ±3
	η	0.3003±0.0007	548±1	0.0[a]	101 ±3
	ω	0.6130±0.0005	783±0.3	15.6±0.2	269 ±3
	ρ	0.59[a]	768[a]	155 ±2	468 ±10
	η'	0.910 ±0.002	954±1	1.7±1	40.5±1
3.71–3.85 (3 GeV; all data)	π	0.0194±0.0006	139±2	0.0[a]	154 ±3
	η	0.3003±0.0006	548±1	0.0[a]	104 ±3
	ω	0.6121±0.0004	782±0.3	11.5±0.2	243 ±3
	ρ	0.59[a]	768[a]	160 ±2	542 ±10
	η'	0.9102±0.0017	954±1	13 ±1	41 ±1
2.8 (2 GeV; all data)	π	0.0182±0.0005	135±2	0.0[a]	1084 ±52
	η	0.2955±0.0005	543±0.5	0.0[a]	790 ±28

[a] Held fixed during fitting routine.

(4) deuterons or heavier particles produced upstream of the target, making He^3's in the target.

All of these mechanisms except possibly (2) produce smooth backgrounds which rise toward smaller angles (i.e., higher masses). Runs taken with hydrogen (instead of deuterium) in the target tend to confirm this rise.

While mechanism (2) is proportional to the number of He^3's passing through the magnet, it may generate angular distributions of these He^3's at a given magnet setting which are not uniform. However, if runs are made at closely spaced magnet angle settings (as were ours), these angular irregularities should average out to a smooth background which rises at smaller angles.

The data which are presented in Table II (and which have been previously published[10]) were based on a preliminary value of the PPA peak machine energy. The calibration of the absolute angle of the spectrometer relative to the external proton beam was also based upon this preliminary value. Analysis of the data showed that this preliminary value of the peak energy was in error. In addition it was discovered that there were also temporal variations in the peak energy. Since this experiment was run in the Jacobian-peak region, there are only two independent kinematic variables required to specify the missing mass (incident proton energy and spectrometer angle). Because three narrow meson states (π, η, and ω) are observed, it is possible to overdetermine these two kinematic variables. It is interesting to note that if there had not been temporal variations in the peak energy of the machine, or if a precise method of monitoring the energy had been used, this experiment would have been able to provide an exceedingly accurate mass value for the third meson state. As it was, however, this technique allowed a measure of this temporal machine energy variation.

The results of the recalibration of the average peak machine energy (13.5-MeV change) and spectrometer angle (0.69-mrad change) lead to the mass values shown in Table III. The values of the π, η, and ω masses obtained by this adjustment now agree with those listed in Ref. 3. The state observed at 953 MeV in the preliminary calculation (Table II and Ref. 10) now appears at 956 MeV, which is in better agreement with the accepted mass of the $\eta'(958)$. No errors are given for the mass values of the π, η, and ω listed in

TABLE III. Cross sections and widths of resonances observed with adjusted values of p_1 and θ_3. Errors shown include systematic effects and normalization error.

Incident proton energy	Meson observed	Mass^2 (GeV^2)	Mass (MeV)	Width (MeV)	$d\sigma/d\Omega$ (10^{-36} cm^2/sr)
3 GeV	π	0.0182	134.9	0	144 ± 36
	η	0.3008	548.4	0	104 ± 26
	ω	0.6145	783.9	11 ± 3	243 ± 62
	ρ	0.59	765		550 ± 250
	η'	0.9145	956.3 ± 2	<20	41 ± 20
2 GeV	π	0.0182	135	0	1084 ± 300
	η	0.297	545	0	790 ± 230

Table III, since the machine energy and angle were adjusted to give the nominal mass values. The error in mass of the η' (±2 MeV) comes from a number of sources, some of which (statistics of the fit, etc.) were included in the previously published paper. A new source of error is the temporal variation in peak machine energy. Analysis of the data taken on the sharp meson states obtained at different times during the run shows a variation in peak energy of ±10 MeV. Because the angular acceptance of the spectrometer was small, it was not possible to observe both the η' and the ω at the same time. Therefore there was no way to determine the machine energy during the η' runs. This temporal variation in machine energy leads to an uncertainty in the mass measurement of the η' enhancement of ±1.6 MeV. This error is added in quadrature to the statistical error (±1 MeV) from the fitting program to yield an over-all estimate of ±2 MeV as the uncertainty in the absolute mass value of the observed peak.

The mass value obtained (956 MeV) and the error assigned (±2 MeV) tend to favor this bump being the $\eta'(958)$, but it does not completely exclude the $M(953)$ (Ref. 11) or the possibility that this enhancement is from both the $\eta'(958)$ and the $M(953)$.

It should be noted that known masses provide an exceptionally precise means of measuring the peak machine energy. We estimate that our absolute error on the peak proton momentum was ±10 MeV/c, or 0.25%.

The division of the data into three momentum intervals provides a very valuable check on the consistency of the fitting routines. A comparison of the fitted masses, widths, and cross sections for the three momentum intervals and for the total data sample permit a crude evaluation of the errors quoted.

The relative magnitudes of all cross sections are strongly influenced by the exact nature of the background upon which the peaks are superimposed. Since the π and η are very narrow, faulty assumptions in the background do not have a large effect unless the background has very large discontinuities. An examination of Table II shows quite satisfactory consistency for the cross sections and errors quoted. The primary source of error in the relative cross sections for the π and the η is thus not from the fitting routine but from the 5% estimated variation in the acceptance of the system.

Although the ω is also very narrow, it is superimposed on a rapidly rising background as well as an indeterminate swelling corresponding to the ρ meson. The fits to the cross section in Table II are not internally consistent, and seem to indicate an error on the order of between 5% and 10%. The fits to the ω width are extremely inconsistent. This inconsistency indicates an error in the width of more than 25%.

The cross section for the ρ meson is extremely sensitive to background assumptions. The great inconsistency in the fitted values of the cross section in Table II is a striking measure of this sensitivity. It is quite clear that an experiment such as this one does not measure the parameters of wide resonances well. The error in the ρ cross section is probably about 30%. The error in the width is at least that large.

Table III includes our estimate of the actual relative errors in the measured parameters. These estimates include contributions from the uncertainty in the relative system acceptance and from the fitting difficulties mentioned above, and include the absolute errors (which are the same for all cross sections at a given proton energy) due to the uncertainties in the absolute intensity of the proton beam, the system acceptance, and counting efficiencies. These latter errors produce an absolute uncertainty in all cross sections of about 25% at 3 GeV and 30% at 2 GeV.

The combination of the fine resolution of the apparatus and the high statistics of the data makes

it possible to place limits on the cross section of bumps which were not seen. From an examination of the mass plot of the averaged 3-GeV data, Fig. 12 D, it is evident that there are no other narrow resonances with cross sections comparable to half that of the η' (i.e., none larger than 20 picobarns/sr) between the major peaks in the mass region covered by the experiment. Limits on cross sections for wider resonances are related to their estimated widths and depend very strongly on the background shape.

The most significant deviation between the data and the best fit is in the region immediately above the 2π threshold. Both the data at 3 GeV and the data at 2 GeV show the same type of departure between the fit and the data. The latter data were taken primarily to investigate this phenomenon with better resolution.

Although the size of the difference between the data and the fit could be changed by modifying some of the background parameters, none of these modifications were sufficient to eliminate the difference. In addition, reasonable assumptions about the validity of the background in this region (see discussion of background, above) do not lead to any obvious method of eliminating the effect, but in fact would enhance it. One of the present authors (H. B.) has published a tentative explanation for the spectra in this region.[12]

The primary advantage of using this type of experiment for a systematic resonance search seems to lie primarily in the very good resolution and statistical accuracy which it provides at masses below about 1 GeV. At high masses, although the resolution is in principle even better, the steeply rising background from multipion production effectively obscures the small cross section for resonant production. Tests at higher proton energies[13] confirm the very steep drop in cross sections with increasing energy. Although the mechanism of this drop is itself very interesting,[12] it does make the use of this method for resonance searches at high energies very unpromising.

ACKNOWLEDGMENTS

We are very grateful for the assistance of Professor R. Schluter, who played a major role in the planning of the experiment and provided much of the equipment necessary for its implementation. Professor F. Shoemaker was very helpful in the early phases of the experiment, and Dr. D. Kreinick was very helpful with the reduction of the data. G. Featherston and D. Hartman provided a great deal of assistance in all phases of the experiment. We are grateful to T. Droege and the members of his electronics group at PPA for designing and building the coding apparatus necessary for the experiment, and for nursing us to an understanding of its operation. Finally, we would like to thank Professor M. G. White and the entire staff of the Princeton-Pennsylvania Accelerator for the very high level of support and cooperation which was provided.

---

*Work supported in part by the U. S. Atomic Energy Commission.

†Now at Rutherford High Energy Laboratory, Chilton, Didcot, Berkshire, England.

‡Work supported in part by National Science Foundation.

§Now at University of Liverpool, P. O. Box 147, Liverpool, England.

‖Now at Upsala College, East Orange, New Jersey.

¶Now at RCA, Heightstown, New Jersey.

[1]M. N. Focacci, W. Kienzle, B. Levrat, B. C. Maglić, and M. Martin, Phys. Rev. Lett. 17, 890 (1966).

[2]R. Baud, H. Benz, B. Bosnjakovic, D. R. Botterill, G. Damgaard, M. N. Focacci, W. Kienzle, R. Klanner, C. Lechanoine, M. Martin, C. Nef, P. Schübelin, and A. Weitsch, Phys. Lett. 30B, 129 (1969). Detailed references to other missing-mass experiments are given in Ref. 3, below.

[3]Particle Data Group, Phys. Lett. 39B, 1 (1972).

[4]A much more detailed discussion of the characteristics of this general method is given by B. Maglić and G. Costa, Phys. Lett. 18, 185 (1965).

[5]A description of an earlier missing-mass detection system which utilized orthogonal measurement of the angle and momentum of the detected particle is given by C. M. Ankenbrandt, A. R. Clark, B. Cork, T. Elioff, L. T. Kerth, and W. A. Wenzel, IEEE Trans. Nucl. Sci. 12, 4, 113 (1965).

[6]A discussion of the focusing properties of the fringe field of a dipole magnet is given by W. Cross, Rev. Sci. Instrum. 22, 717 (1951).

[7]The cross sections shown in Figs. 10–12 and in Table II are twice as large as those presented in a previous preliminary report on this experiment [H. Brody *et al.*, Phys. Rev. Lett. 24, 948 (1970)]. This earlier paper utilized an acceptance for the apparatus which was twice as large as that obtained when efficiencies and the momentum acceptance of the system were more carefully examined. In addition, the vertical scale on Fig. 1 of this earlier paper should have read from 1.0 to 5.0 ($\times 10^{-33}$ cm^2/sr GeV^2) rather than from 0.1 to 0.5 ($\times 10^{-33}$ cm^2/sr GeV^2).

[8]R. Hagedorn, *Relativistic Kinematics* (Benjamin, New York, 1964).

[9]J. D. Jackson, Nuovo Cimento 34, 1644 (1964).

[10]B. Maglich, J. Oostens, M. Silverman, H. Brody, G. Featherston, E. Groves, R. Van Berg, W. Wales, G. B. Cvijanovich, and D. Hartman, Phys. Rev. Lett.

27, 1479 (1971).
[11]M. Aguilar-Benitez, D. Bassano, R. L. Eisner, J. B. Kinson, D. Pandoulas, N. P. Samios, and V. E. Barnes, Phys. Rev. Lett. 25, 1635 (1970).
[12]H. Brody, Phys. Rev. Lett. 28, 1217 (1972).
[13]A test run at the ZGS indicated that the cross sections for η and ω production using 5-GeV protons were significantly lower than the cross sections reported here. See R. A. Schluter, P. M. Patel, C. Rippich, D. G. Ryan, F. Sannes, D. G. Stairs, J. M. Trischuk, and H. Brody, Nucl. Phys. B60, 396 (1973).

PHYSICAL REVIEW D VOLUME 9, NUMBER 7 1 APRIL 1974

Search for massive long-lived particles in aluminum targets irradiated by 300- and 400-GeV protons*

S. Frankel, W. Frati, L. Resvanis, and W. Yang
Department of Physics, University of Pennsylvania, Philadelphia, Pennsylvania 19174

F. Nezrick
National Accelerator Laboratory, Batavia, Illinois 60510
(Received 15 October 1973)

We have used a directional gas Cherenkov counter, which employed six phototubes to sample Cherenkov light from single particles having a γ [$\equiv (1-v^2/c^2)^{-1/2}$] greater than ~ 10, to achieve accidental rates of less than one per day if operated near targets with surface radiation levels of as high as 10^{+3} R/h. The cosmic-ray background measured by our apparatus was reduced to less than one per day by mounting our directional Cherenkov counter above the irradiated targets and facing toward the earth. Two searches of a few days' duration, after bombardments at energies of 300 and 400 GeV with $> 10^{16}$ protons at NAL, were made in 4-in.-thick targets of aluminum mounted just downstream from another aluminum target. No long-lived particles were observed with cross sections for production and capture of approximately less than a picobarn in a lifetime range of a few to a few thousand hours.

I. INTRODUCTION

Whenever a new energy range is opened up for experimental investigation by the design and construction of a new high-energy accelerator it is of interest to carry out searches for new and unpredicted particles. This paper describes the negative results of a search for new massive long-lived particles produced in thick aluminum targets by 300- and 400-GeV protons at the National Accelerator Laboratory.

Unlike the antiproton (and the postulated but unobserved particles such as the quark, magnetic monopole, and intermediate vector boson) strange particles were unpredicted particles. Had they not possessed the new strangeness quantum number they would have decayed via the strong interaction with extremely short lifetimes and have been exceedingly difficult to detect. On the other hand, had strangeness been rigorously conserved, these new particles would have been stable. Forbidden to decay electromagnetically, but as it turned out not forbidden to decay via the weak interaction, these particles, violating strangeness in their decay, turned out to have lifetimes of the same order of magnitude as previously observed strangeness-conserving weak decays.

There is no reason to believe that the creation of new particles possessing new quantum numbers, and decaying by the violation of some new symmetry, will recur at higher energies, but it was this hope that prompted the search for long-lived particles described in this note.[1]

Because of the small probability of finding new and unpredicted particles this experiment was designed to adhere to certain constraints: that it be carried out with little cost and effort, with available equipment, and that it be parasitic in nature.

The basic purpose of the experiment was to search for the decay of massive particles of long half-life. Our aim was to achieve a sensitivity of a few decays per day in the presence of cosmic-ray background and in the presence of the high levels of radioactivity expected in targets irradiated with $\geq$300-GeV protons at NAL.

To do so we chose to look for decay modes of these heavy particles which would ultimately lead